



## OPEN ACCESS

## EDITED BY

Guozhu Li,  
Chinese Academy of Sciences (CAS), China

## REVIEWED BY

Prayitno Abadi,  
Indonesian National Research and Innovation  
Agency (BRIN), Indonesia  
Tulasiram Sudarsanam,  
Indian Institute of Geomagnetism (IIG), India

## \*CORRESPONDENCE

Chunhua Jiang,  
✉ chuajiang@whu.edu.cn  
Tongxin Liu,  
✉ tongxin\_liu@whu.edu.cn

RECEIVED 25 November 2025

REVISED 26 January 2026

ACCEPTED 02 February 2026

PUBLISHED 18 February 2026

## CITATION

Zhao Z, Zhu L, Jiang C, Liu T, Yang G and  
Zhao Z (2026) Modeling the effects of  
equatorial plasma bubbles on the oblique  
propagation of high-frequency  
electromagnetic waves.  
*Front. Astron. Space Sci.* 13:1753973.  
doi: 10.3389/fspas.2026.1753973

## COPYRIGHT

© 2026 Zhao, Zhu, Jiang, Liu, Yang and Zhao.  
This is an open-access article distributed  
under the terms of the [Creative Commons  
Attribution License \(CC BY\)](#). The use,  
distribution or reproduction in other forums is  
permitted, provided the original author(s) and  
the copyright owner(s) are credited and that  
the original publication in this journal is cited,  
in accordance with accepted academic  
practice. No use, distribution or reproduction  
is permitted which does not comply with  
these terms.

# Modeling the effects of equatorial plasma bubbles on the oblique propagation of high-frequency electromagnetic waves

Ziyi Zhao<sup>1</sup>, Lingyun Zhu<sup>1</sup>, Chunhua Jiang<sup>1\*</sup>, Tongxin Liu<sup>1\*</sup>,  
Guobin Yang<sup>1</sup> and Zhengyu Zhao<sup>1,2</sup>

<sup>1</sup>School of Earth and Space Science and Technology, Wuhan University, Wuhan, China, <sup>2</sup>Institute of Space Science and Applied Technology, Harbin Institute of Technology, Shenzhen, China

The ionosphere, as an essential component of the Earth's space environment, contains free electrons that influence the amplitude and phase of radio signals. In the equatorial and low-latitude regions, plasma bubbles in the F region, manifested as electron density depletion, are observed frequently during the postsunset period. This phenomenon severely impacts the performance of modern electronic systems, such as short-wave communications and satellite navigation systems. In short-wave communication and target localization systems, the propagation mode of high-frequency electromagnetic waves in the ionosphere is typically oblique propagation. Therefore, studying the effects of equatorial plasma bubbles (EPB) on the oblique propagation characteristics of short waves is of significant engineering application importance. In this study, first, a model of plasma bubbles was used to produce equatorial plasma bubbles in the ionosphere. Then, a ray-tracing method was utilized to simulate the oblique propagation of radio waves in the ionosphere and synthesize oblique ionograms. Finally, the influence of EPB on the morphology of oblique ionograms was investigated, and the synthesized ionograms were compared with the measured oblique ionogram. Results showed that the features of the echoes such as satellite traces in the low working frequency band and diffuse echoes in the high working frequency band could be well reproduced in the simulated oblique ionograms, and that EPB could cause severe spread in both the group path and frequency of the high working frequency band of oblique ionograms, which was highly similar to the characteristics of spread F in the measured ionograms.

## KEYWORDS

high-frequency oblique propagation, oblique ionogram, plasma bubbles, satellite trace, spread F

## 1 Introduction

The ionosphere, located 60 km–1,000 km above the Earth's surface, is a region of the atmosphere where neutral atmospheric particles are partially ionized. The electron density in this region varies dynamically with altitude, latitude, day and night, and solar

activity, and it is a key medium for the long-distance propagation of high-frequency (HF) electromagnetic (EM) waves (3 MHz–30 MHz) (Kelley, 2009). HF waves can propagate over thousands of kilometers by reflecting off the F layer of the ionosphere, which is widely used in emergency communications, over-the-horizon radar target monitoring, and space weather observation. However, in equatorial and low-latitude regions, plasma bubbles are frequently observed at the bottom of the ionospheric F layer at night, which is attributed to Rayleigh-Taylor instability. These irregularities can cause the deflection of the propagation path of radio waves, signal amplitude and phase scintillations, and significantly degrade the performance of short-wave communication and radar systems (Dungey, 1956; Ossakow, 1981). Therefore, studying the effects of equatorial plasma bubbles (EPB) on the oblique propagation of HF radio waves is of great practical significance for ensuring the reliability of short-wave communication and radar systems. Moreover, shortwave communication and radar detection mostly adopt the mode of high-frequency radio wave oblique propagation, which shares highly similar propagation mechanisms with ionospheric oblique sounding. Oblique ionograms can accurately capture key perturbation characteristics such as low-frequency satellite traces and high-frequency spread F during the development of plasma bubbles, providing direct ionospheric environment reference for users of shortwave communication systems. Therefore, this study has significant value for shortwave communication systems and engineering applications of radar detection.

Research on plasma bubbles in equatorial and low-latitude regions began in the 1930s. Booker and Wells first observed the spread F at night in the equatorial region and proposed that ionospheric irregularities are the main cause of radio wave scattering (Booker and Wells, 1938). Later, Dungey proposed the Rayleigh-Taylor instability to explain the formation mechanism of plasma bubbles in the equatorial region (Dungey, 1956). Fejer and Kelley further proposed the generalized Rayleigh-Taylor (GRT) instability by considering the effects of electric fields and neutral winds, thus improving the physical understanding of ionospheric plasma bubbles evolution in equatorial and low-latitude regions (Fejer and Kelley, 1980). With the understanding of the physical mechanisms of ionospheric plasma bubbles, significant progress was made in the simulations and models of plasma bubbles. Many scholars have conducted research on two-dimensional models of ionospheric plasma bubbles (Alam et al., 2004; Huang and Kelley, 1996; Huba and Joyce, 2007; Zalesak and Ossakow, 1980; Zalesak et al., 1982). In recent years, three-dimensional numerical models of ionospheric plasma bubbles have also been developed (Huba et al., 2008; Yokoyama et al., 2014; Li et al., 2023).

In the simulation of radio wave propagation, the ray-tracing method has become one of the primary tools for studying ionospheric wave propagation due to its ability to intuitively describe the relationship between wave traces and medium parameters. Paul et al. used the ray-tracing method to synthesize ionograms perturbed by sulfur hexafluoride (SF<sub>6</sub>), verifying the applicability of this method to perturbed ionosphere (Paul et al., 1968). Mathur and Pandey, by artificially constructing the equations of ionospheric irregularities, used the ray-tracing method to investigate the effects of ionospheric irregularities on HF and very high-frequency (VHF)

radio waves propagation (Mathur and Pandey, 1977). Various ray-tracing programs were developed by researchers (Song et al., 2022; Haselgrove, 1963; Jiang et al., 2019; Cervera and Harris, 2014; Jones, 1968; Jones and Stephenson, 1975). Cervera and Harris, based on Haselgrove's related work (Haselgrove, 1963), developed the short-wave ray-tracing program (PHaRLAP) (Cervera and Harris, 2014), which can run ray-tracing methods in both two-dimensional and three-dimensional coordinate systems. In recent years, Jiang et al. have used the ray-tracing method to simulate spread F in vertical ionograms and studied the effects of ionospheric plasma bubbles on vertical ionograms (Jiang et al., 2020).

Vertical sounding is a classic ionospheric detection method, whose detection mode is illustrated in the left figure (a) of Figure 1. By transmitting radio waves vertically upward from the ground directly below the target area and receiving the returned signals from the reflection of the ionosphere at the same location. The ionosphere sounding system can record the time delay of radio wave reflection at different working frequencies. The schematic diagram of oblique sounding is shown in the right figure (b) of Figure 1. This detection method adopts a two-station cooperative mode, where the transmitter and receiver are placed separately at two locations with a certain distance apart. The transmitter transmits radio detection signals obliquely upward, which are captured by the receiver at the other location after being reflected by the ionosphere. By measuring the group delay of signals at each frequency point, the oblique ionogram can be obtained, realizing the detection of the ionosphere over a range of thousands of kilometers.

Currently, research on ionospheric plasma bubbles is predominantly focused on vertical detection, and there is a paucity of studies on how plasma bubbles affect the oblique propagation of high-frequency radio waves and the morphological changes of oblique ionograms. Ankita et al. investigated the effects of ionospheric upwelling and plasma bubbles on satellite traces and vertical incidence ionograms (Ankita et al., 2025); Ma et al. used the three-dimensional ray-tracing method to establish a 3D model of EPB with different scales, times, and heights, and simulated and analyzed its influence on the propagation paths of HF radio waves under the scenario of vertical incidence at low latitudes (Ma et al., 2023). In this study, we investigated the effects of EPB on the morphological changes of oblique ionograms and compared these results with measured oblique ionograms.

## 2 Model of ionospheric plasma bubbles

In this study, we utilized the two-dimensional model of plasma bubbles developed by Jiang and Zhao (2019), and Jiang et al. (2023) to simulate ionospheric plasma bubbles. This model is based on fluid dynamics theory and took into account electron and ion transport processes, recombination effects, and gravity field influences. The model equations are given by Equations 1–3:

1. Continuity Equation:

$$\frac{\partial N_{e,i}}{\partial t} + \nabla \cdot (N_{e,i} \mathbf{V}_{e,i}) = -\nu_R(N_{e,i} - N_0) \quad (1)$$

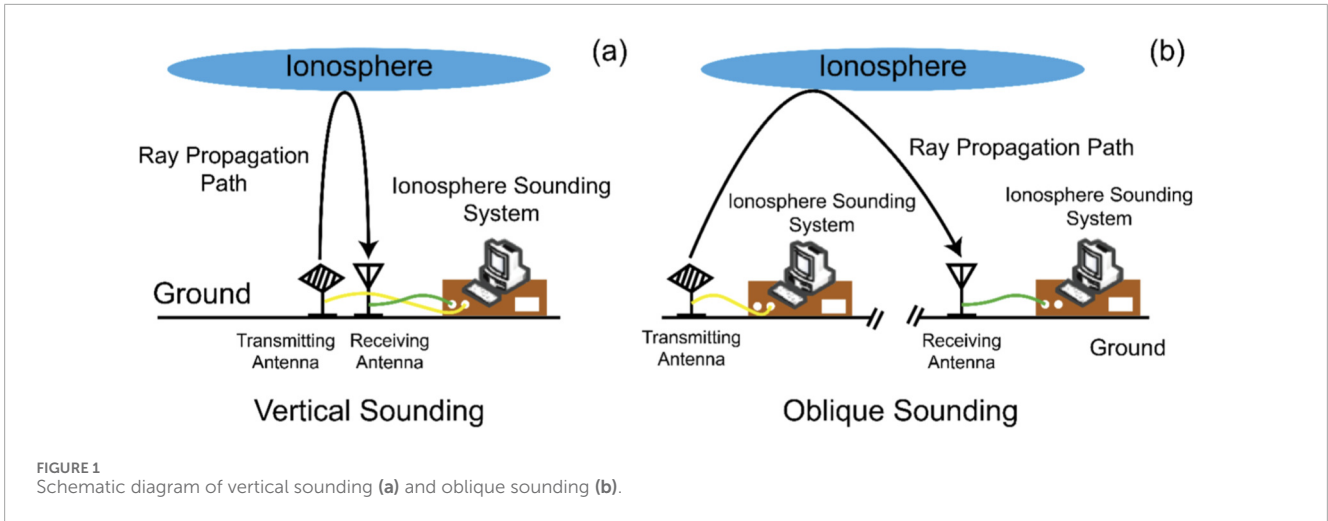


FIGURE 1 Schematic diagram of vertical sounding (a) and oblique sounding (b).

where  $N_{e,i}$  represents the density of electrons or ions;  $N_{e,i} = N_e = N_i$  under quasi-neutrality condition;  $t$  is the simulation running time;  $V_{e,i}$  represents the velocity of electrons or ions;  $\nu_R$  is the recombination coefficient, and  $N_0$  represents the initial electron density. This equation describes the time evolution of the density of electrons or ions as well as convective transport and the ionization-recombination process.

2. Electron and Ion Momentum Equation:

$$N_{e,i}M_{e,i}\left(\frac{\partial}{\partial t} + V_{e,i} \cdot \nabla\right)V_{e,i} = qN_{e,i}(E + V_{e,i} \times B) + N_{e,i}M_{e,i}g + M_{e,i}u_{en,in}(U - V_{e,i}) \tag{2}$$

where  $M_{e,i}$  represents the mass of the electron or ion;  $V_{e,i}$  represents the velocity of electron or ion;  $q$  is the charge;  $E$  is the electric field,  $E = E_0 - \nabla\phi$ ;  $E_0$  and  $\phi$  represent the background electric field and electrostatic polarization potential respectively;  $B$  refers to the geomagnetic field;  $g$  represents gravitational acceleration;  $u_{en,in}$  represents the collision frequency of electrons and ions with neutral particles, and  $U$  denotes the neutral wind speed. This equation is used to describe the variation in electron or ion momentum, balancing electromagnetic (EM) force, gravity, and electron-neutral particle collision force or ion-neutral particle collision force.

3. Current Continuity Equation:

$$\nabla \cdot J = \nabla \cdot [q(N_iV_i - N_eV_e)] \tag{3}$$

where  $J$  represents the total current density. Based on the charge conservation law, this equation indicates that there is no net charge accumulation in the ionosphere, and the divergence of the current density is zero, ensuring the consistency between the electric field and particle motion.

In this study, the numerical calculations were performed on the two-dimensional Cartesian coordinate system  $(X,Z)$ , where  $X$  represented the vertical direction (km) and  $Z$  represented the zonal direction (km). The number of grid points was 451 in the vertical direction ( $X$ ) and was 501 in the zonal direction ( $Z$ ). The grid

spacing in both directions was 2 km. The model region spanned an altitude range of 100 km–1,000 km and a zonal range from 0 km to 1,000 km. The geographic longitude was 100°, the latitude was 10°, and the azimuth was 90°. Additionally, solar activity and geomagnetic background parameters were inputted, with F10.7 = 120, F10.7A = 120, and AP = 3. In the simulation of the ionospheric plasma bubbles, the initial perturbation source was modeled as a sinusoidal perturbation. For simplicity, in this study, neutral wind was neglected ( $U = 0$ ) to focus on the evolution of plasma bubbles. The simulation started at 7:00:00 on 20 March 2016 (local time 14:00:00), with the initial perturbation set at 20:00 local time.

### 3 Simulation of oblique ionogram

The propagation path of radio waves through the ionospheric medium is given by Equation 4 (Kudeki, 2010):

$$\begin{cases} \frac{dk}{d\tau} = \frac{1}{2} \frac{\omega}{c} \nabla n^2 \\ \frac{dr}{d\tau} = \frac{c}{\omega} k \end{cases} \tag{4}$$

where  $k$  is the wave number;  $r$  is the wave vector;  $\tau$  represents the group path of radio waves;  $\omega$  is the angular frequency of radio waves;  $c$  is the speed of light in a vacuum, and  $n$  is the refractive index of the ionosphere. The refractive index  $n$  in the ionosphere is determined by the electron density, and when the geomagnetic field is neglected, it is expressed by Equation 5:

$$n = \sqrt{1 - 80.6N(h)/f^2} \tag{5}$$

where  $N(h)$  is the electron density at height  $h$ , and  $f$  is the frequency of radio waves.

In this study, the PHaRLAP tool (Cervera and Harris, 2014) was used to simulate the propagation of radio waves through the ionosphere. The ionospheric environment was modeled using the ionospheric plasma bubble model introduced in this study, which not only simulates the formation of plasma bubbles but also accounts for the diurnal variation of the ionosphere. In the PHaRLAP tool, the

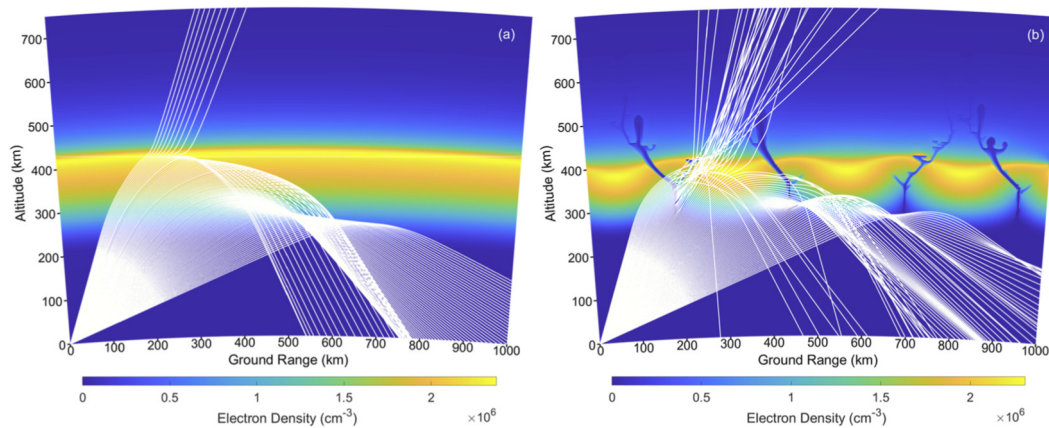


FIGURE 2 Propagation paths of radio waves with the frequency of 15 MHz in the ionosphere without (a) and with (b) plasma bubbles.

group path is calculated by Equation 6 (Cervera and Harris, 2014):

$$P^l = \int \mu^l \cos \alpha dl \tag{6}$$

where  $\alpha$  is the angle between the wave normal and the ray direction, and  $\mu^l$  is the group refractive index. The angle  $\alpha$  can be calculated by Equation 7 during the numerical integration:

$$\cos \alpha = \frac{\vec{k} \cdot \vec{r}}{\mu \cdot |\vec{r}|} \tag{7}$$

The relationship between the group refractive index  $\mu^l$  and the refractive index  $\mu$  is given by Equation 8:

$$\mu^l = \frac{d(\mu f)}{df} \tag{8}$$

where  $f$  is the frequency of radio waves.

## 4 Results and discussion

Figure 2 shows the propagation of radio waves with a frequency of 15 MHz in the ionosphere before and after perturbation. The elevation angle of radio waves was between 20° and 70°, with a step of 0.5°. In Figure 2, the white solid lines represent the propagation path of radio waves. The left figure (a) in Figure 2 shows the propagation of radio waves in the ionosphere without equatorial plasma bubbles (EPB), where the ray distribution is uniform, and the propagation path is orderly and continuous. The right figure (b) in Figure 2 shows the propagation of radio waves in the ionosphere containing EPB. Due to the influence of plasma bubbles, the ray propagation paths become complex and scattered, exhibiting significant perturbation features. Therefore, the presence of plasma bubbles leads to a noticeable alteration in the propagation path of radio waves.

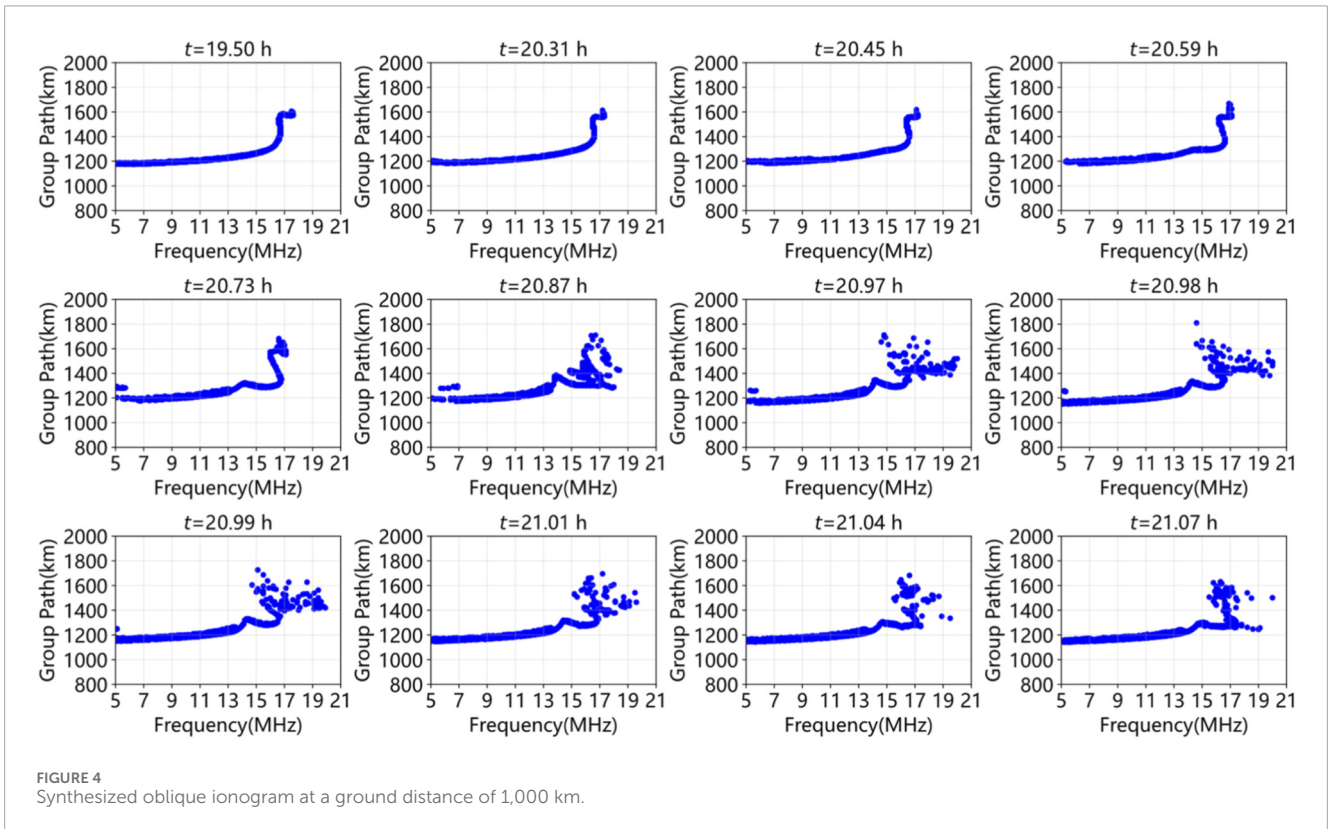
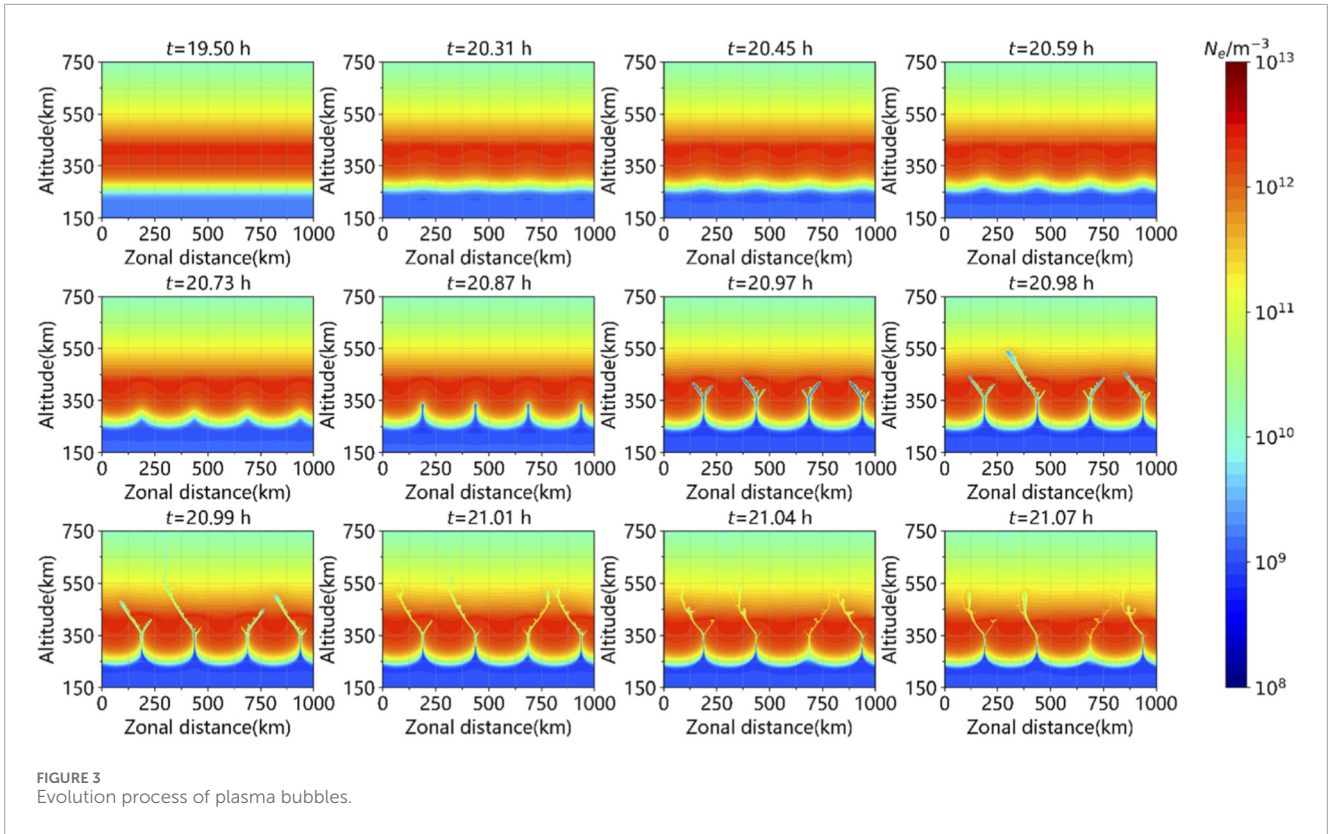
To study the effects of plasma bubbles on oblique ionograms, Figure 3 shows the evolution process of plasma bubbles. The time range was from  $t = 19.50$  h to  $t = 21.07$  h, with the x-axis representing the zonal distance (km) and the y-axis representing the altitude (km). The color bar represented the magnitude of electron

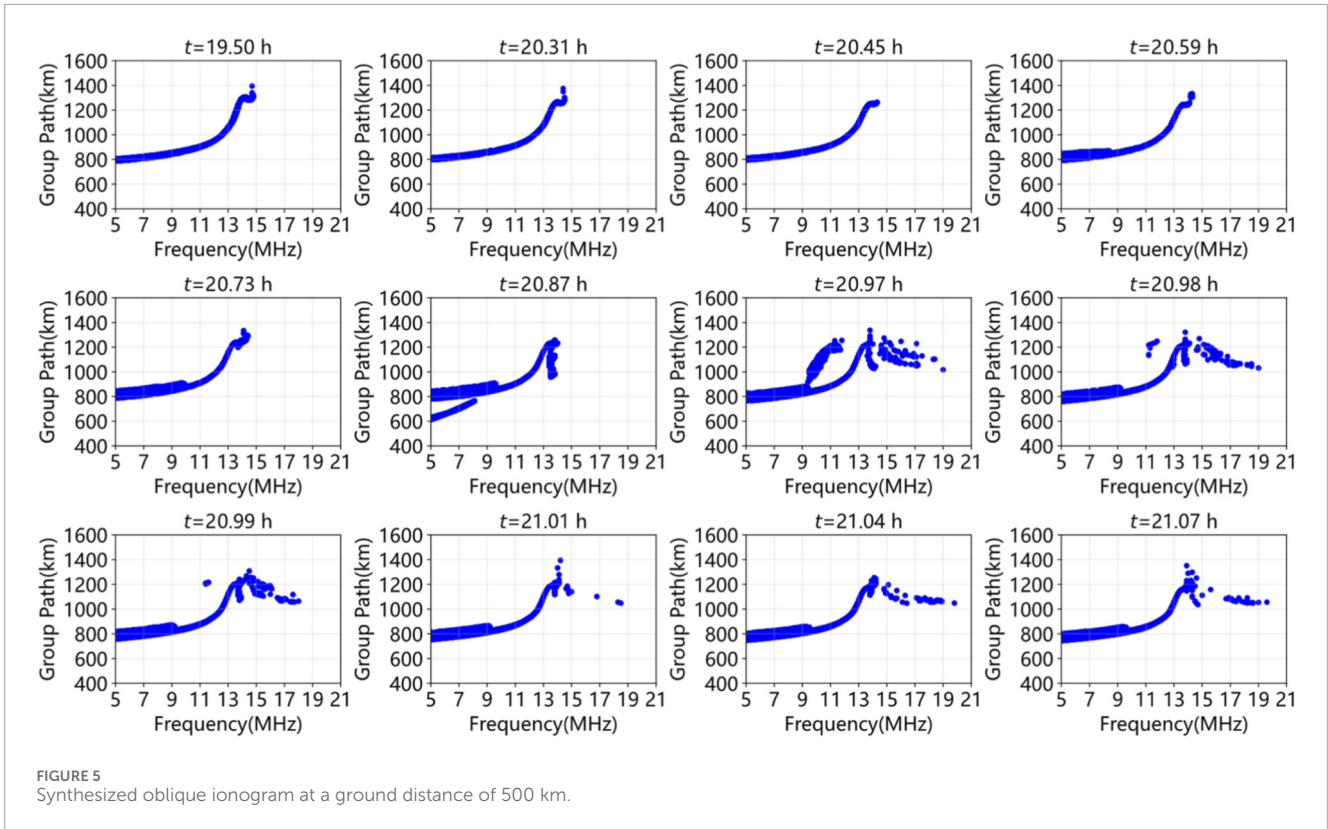
density ( $10^8 \text{ m}^{-3}$  to  $10^{13} \text{ m}^{-3}$ ), with all subplots using a unified scale. Based on the evolution process, the formation and development of plasma bubbles could be divided into three stages:

1. Initial Quiet Stage ( $t = 19.50$  h–20.31 h): The electron density distribution in the ionosphere was uniform, with no significant low-density regions, indicating that the sinusoidal perturbation had not yet triggered plasma bubbles.
2. Formation Stage ( $t = 20.59$  h–20.87 h): At  $t = 20.59$  h, low-density points appeared in the 250 km altitude region, indicating the beginning of the formation of plasma bubbles. As time progressed, the low-density region gradually expanded into a continuous strip-like structure, extending upward to 350 km, indicating that plasma bubbles were growing under the influence of the sinusoidal perturbation.
3. End Stage ( $t = 20.97$  h–21.07 h): After  $t = 20.97$  h, plasma bubbles exhibited bifurcation and expansion characteristics. Some bubbles split into multiple smaller ones, while others penetrated to higher altitudes. From  $t = 20.98$  h to  $t = 21.01$  h, the spatial coverage of plasma bubbles reached its maximum, and the electron density gradient was at its highest. From  $t = 21.04$  h to  $t = 21.07$  h, the low-density regions began to contract, and the electron density gradient decreased, indicating that the plasma bubbles had entered the decay phase.

In this study, based on the evolution process of plasma bubbles in Figure 3, we used the ray-tracing method to synthesize oblique ionograms for ground distances of 1,000 km (Figure 4) and 500 km (Figure 5). In the simulations of the oblique ionograms at two different ground distances, the working frequency range of radio waves was from 5 MHz to 20 MHz, with a step of 0.1 MHz, and the elevation angle of radio waves was 20°–70° (1,000 km) and 30°–65° (500 km).

Figure 4 shows the oblique ionogram for a ground distance of 1,000 km. At  $t = 20.73$  h, satellite traces (Tsunoda, 2008) (which are one or more accompanying traces on the ionogram that resemble the main trace but differ slightly in group path when there are small-scale perturbations in the ionosphere, before spread F occurs) began





to appear in the low working frequency band (5 MHz–8 MHz), and satellite traces disappeared after  $t = 20.99$  h. At  $t = 20.87$  h, the group path and frequency in the high working frequency band (15 MHz–20 MHz) began to show the characteristics of diffuse spread F, which coincided with the time when the plasma bubbles started to significantly penetrate upward at  $t = 20.73$  h in Figure 3. As time progressed, the spread of the traces gradually expanded, the frequency coverage extended from 13 MHz to 20 MHz, and the group path extended from 1,300 km to 1800 km. At  $t = 20.99$  h, spread F reached its maximum, corresponding to the stage in Figure 3 when plasma bubbles exhibited the maximum spatial coverage and the electron density gradient reached its maximum. At this point, the degree of perturbation to radio waves was most significant. After  $t = 21.01$  h, the dispersion degree of the traces gradually decreased, and spread F showed a decreasing trend, which was consistent with the trend observed in Figure 3 when plasma bubbles began to contract and the electron density gradient decreased at  $t = 21.01$  h.

Figure 5 shows the oblique ionogram for a ground distance of 500 km which exhibits a similar evolutionary trend for spread F, consistent with Figure 4. In Figure 5, the diffuse spread F characteristics began to appear at  $t = 20.87$  h and underwent an evolutionary process of “emergence–strengthening–weakening”. Additionally, Figure 5 first shows satellite traces at  $t = 20.59$  h, while Figure 4 shows satellite traces starting at  $t = 20.73$  h. In terms of the duration of satellite traces, in Figure 5, the satellite traces persisted until  $t = 21.07$  h, whereas in Figure 4, satellite traces disappeared from the ionogram starting at  $t = 21.01$  h.

Therefore, based on the sequential oblique ionograms for the growth phase of plasma bubbles, it can be concluded that the degree of influence of plasma bubbles on high-frequency oblique radio wave propagation is significantly correlated with the scale evolution of plasma bubbles. During the initial development stage of plasma bubbles, the plasma bubbles are mainly characterized by the overall expansion of large-scale low-density regions, and small-scale irregular structures have not yet formed. At this time, radio wave propagation is only subject to minor perturbations, manifested as the initial appearance of weak satellite traces, with no obvious diffusion phenomenon in the high-frequency band. This indicates that the deflection effect on radio wave propagation paths and the impact on signal distortion caused by large-scale irregularities are limited.

As plasma bubbles enter the formation and maturation stages, their spatial structure gradually differentiates, exhibiting small-scale irregular features such as “bifurcation and expansion”. The perturbations on radio wave propagation are significantly enhanced, and the spread F appears in the high-frequency band. Moreover, the discrete range of traces gradually widens over time. This indicates that after plasma bubbles develop to the stage where small-scale irregularities emerge, the influence of plasma bubbles on radio wave propagation paths becomes increasingly significant.

By comparing the synthesized oblique ionograms at different times in Figures 4, 5, it can be observed that when the distance between the transmitter and receiver is closer, the satellite traces are earlier and stronger.

The left figure (a) and the right figure (b) in Figure 6 show the propagation paths of 6 MHz radio wave rays in the ionosphere

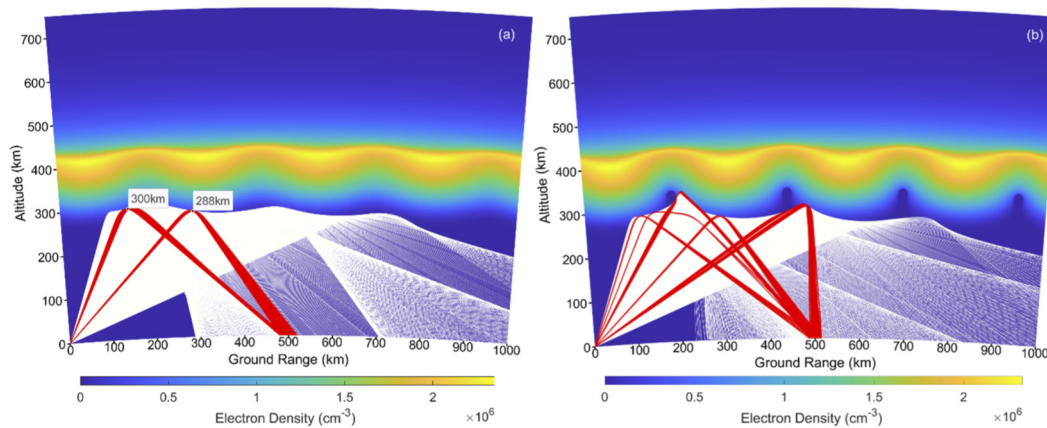


**FIGURE 6** Propagation paths of radio waves with the frequency of 6 MHz in the ionosphere at  $t = 20.59$  h (a) and  $t = 20.87$  h (b). Red lines represent the rays received at locations with a ground distance of  $500 \pm 15$  km.

at  $t = 20.59$  h and  $t = 20.87$  h, respectively, where the red rays correspond to the received rays within the ground distance range of  $500 \pm 15$  km. As shown in the figure, at both time nodes, rays from different ranges of initial elevation angles are received in the  $500 \pm 15$  km region. Thus, satellite traces appear in the 6 MHz band of the synthesized oblique ionograms corresponding to the ground distance of 500 km at both  $t = 20.59$  h and  $t = 20.87$  h. The difference is that  $t = 20.87$  h (Figure 6B) corresponds to the further expansion and evolution stage of plasma bubbles. Affected by the multipath propagation effect of radio waves induced by ionospheric tilting structures, the ray paths become more complex and dispersed, and more rays from different ranges of initial elevation angles converge in the region with a ground distance of  $500 \pm 15$  km, making the satellite trace characteristics more prominent in the ionogram.

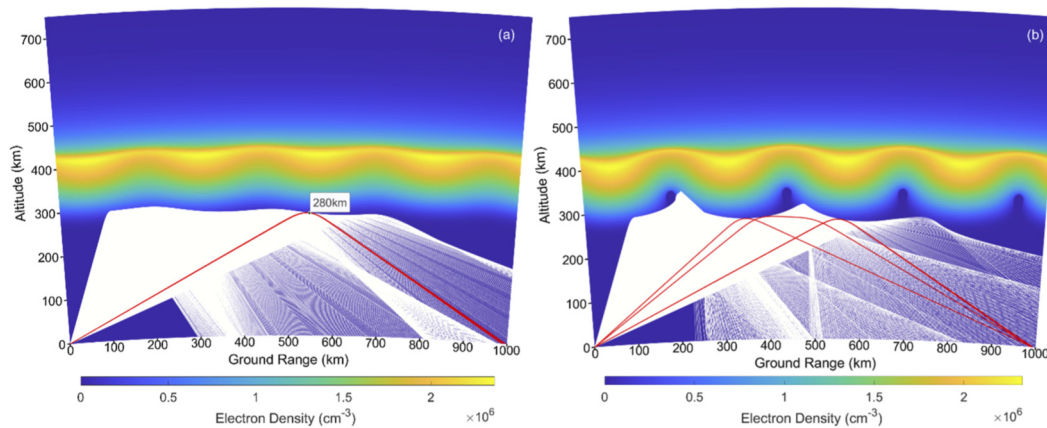
The left figure (a) and the right figure (b) in Figure 7 show the propagation paths of 6 MHz radio wave rays in the ionosphere at  $t = 20.59$  h and  $t = 20.87$  h, where the red rays correspond to the received rays within the ground distance range of  $1,000 \pm 15$  km. At  $t = 20.59$  h (Figure 7a), only rays from a single range of initial elevation angles are received in the  $1,000 \pm 15$  km region, so no satellite traces are observed in the corresponding synthesized oblique ionogram; while at  $t = 20.87$  h (Figure 7b), rays from different ranges of initial elevation angles are received in this region, and satellite traces appear in the ionogram.

Figure 6a shows that at  $t = 20.59$  h, the receiver located at a ground distance of 500 km captures multiple rays propagating along different paths. In contrast, at the same moment, the receiver located at a ground distance of 1,000 km only captures rays within a single elevation range, as shown in Figure 7a. From the perspective of the mechanisms of ionospheric physics and radio wave propagation, after the ionosphere is perturbed, plasma bubbles exhibit evolutionary characteristics of gradual expansion toward the surrounding regions. The formation of satellite traces depends on the oblique reflection of radio waves by ionospheric tilting structures, and there is a correlation between the altitude of ionospheric tilting and the ground propagation distance of the reflected waves. When the distance between the transmitter and receiver is relatively close,

the receiver is more likely to capture high-elevation echoes, which correspond to a high reflection altitude. As indicated in Figure 6a, the features of the ionospheric tilting above an altitude of 300 km are more pronounced. Radio waves propagating in this region tend to induce the multipath effect, thereby generating satellite traces in the ionogram. On the contrary, when the distance of transmitter and receiver is long, the received echoes have a low elevation angle and a corresponding low reflection altitude, which fail to cover the region where the ionospheric tilting structures are located, thus unable to form satellite traces. Therefore, when the distance between the transmitter and receiver is closer, satellite traces appear earlier on the ionogram.

Figure 6b shows that at  $t = 20.87$  h, the rays captured by the receiver located at a ground distance of 500 km from different propagation paths are more densely distributed; while in Figure 7b at the same time, the rays captured by the receiver located at a ground distance of 1,000 km are relatively sparse. In the process of high-frequency radio wave oblique propagation in the ionosphere, the intensity of satellite traces is mainly determined by the propagation geometric effect. Under the influence of the propagation geometric effect, the landing points of rays reflected by the ionosphere with irregularities tend to be concentrated in the region closer to the transmitter. This enables the short-distance receiver to capture more overlapping multipath reflected rays, resulting in a denser ray distribution. In contrast, the ray landing points in the region where the long-distance receiver is located are relatively scattered, the number of rays per unit space is significantly reduced, and the ray distribution is relatively sparse. Therefore, when the distance between the transmitter and receiver is closer, satellite traces exhibit stronger intensity characteristics.

Satellite traces refer to one or more secondary traces that appear at positions with deviated virtual heights on ionograms and are highly similar in morphology to the F-layer main trace. Their essence is the multipath propagation effect of radio waves induced by ionospheric tilting during the early evolutionary stage of plasma bubbles. In this study, during the initial stage of ionospheric perturbation, plasma bubbles are not yet fully developed and only



**FIGURE 7** Propagation paths of radio waves with the frequency of 6 MHz in the ionosphere at  $t = 20.59$  h (a) and  $t = 20.87$  h (b). Red lines represent the rays received at locations with a ground distance of  $1,000 \pm 15$  km.

manifest as ionospheric tilting with large-scale wavy structures in the low-altitude region. When low-frequency radio waves propagate to the low-altitude region, in addition to undergoing normal reflection at the main reflection altitude of the F layer to form the main trace, some radio waves incident on the tilted electron density isosurfaces and undergo oblique reflection, leading to deflection of propagation paths and the formation of multiple reflected signals with the same frequency but different propagation paths. Ultimately, these echoes from different paths are captured by the ground receiver, which are reflected as satellite traces deviated from the main trace in virtual height in the low-frequency band on the synthesized ionogram. Since the transmission and reception of vertical sounding signals are at the same location, while the transmitter and receiver of oblique sounding are located at different locations far apart, the satellite traces obtained by oblique sounding manifest as differences in group distance but maintain similar morphology, in contrast to those commonly observed in vertical sounding. The left figure (a) in Figure 8 shows the propagation paths of low-frequency radio waves in the ionosphere at  $t = 20.97$  h. As shown in the figure, rays from different ranges of initial elevation angles, during their propagation, are affected by the multipath propagation effect induced by ionospheric tilting structures and are all reflected to the region near a ground distance of 500 km. Eventually, these rays manifest as satellite traces in the synthesized ionogram.

Spread F is an observational feature characterized by continuous diffuse broadening of F-layer echoes in ionograms. Its essence is the multipath propagation effect caused by the interaction between plasma bubbles and radio waves, and its formation depends on maturely developed plasma bubbles in the high-altitude region of the ionosphere. In the high-frequency band, the formation of the spread F stems from the stronger penetration capability of high-frequency radio waves, which can reach the high-altitude region above 350 km where plasma bubbles are maturely developed with more irregular structures. After the incidence of high-frequency radio waves, due to the inhomogeneous reflection of plasma bubbles, multiple reflected signals with differences in propagation time and paths are generated. After these radio waves are received by the

ground receiver, they are ultimately reflected as continuous diffuse echo broadening around the F-layer main trace in the ionogram, which corresponds to the spread F in the high-frequency band. The right figure (b) in Figure 8 shows the propagation paths of high-frequency radio waves in the ionosphere at  $t = 20.97$  h. As shown in the figure, high-frequency rays from different ranges of initial elevation angles, during their propagation, are affected by the multipath propagation effect induced by irregular structures in mature plasma bubbles at high altitudes. These rays form multiple reflected signals with distinct propagation times and paths and are reflected to the region near a ground distance of 500 km, eventually manifesting as the spread F in the high-frequency band on the synthesized ionogram.

To verify the reliability of the synthesized oblique ionograms, in this study, Figure 4 is compared with the measured oblique ionogram (Figure 9) from Digital Oblique Receiving System (DORS), which was developed by the Defence Science and Technology (DST) Group of Australia (Ayliffe et al., 2019). Figure 9 was recorded at 14:52:47 on 15 August 2015, with a ground distance of 1,495 km.

From the comparison, the consistency between the synthesized and measured ionograms is evident in two main aspects:

1. Frequency Distribution of Spread F: Both ionograms exhibit spread F in the high working frequency band (exceeding the maximum usable frequency for oblique ionograms), with consistent frequency distribution characteristics. The satellite traces also appear in the low working frequency band.
2. Trace Morphology: The spread F regions exhibit a “diffuse pattern”, without obvious single continuous traces, which is consistent with the signal characteristics of multipath radio wave superposition.

In addition, spread F occurs across the entire frequency band in the measured ionogram, while it only appears in the high-frequency band in synthesized ionograms. The main reasons for this discrepancy are reflected in the following three aspects:

1. As a numerical simulation method, ray-tracing adopts finite discrete elevation angle steps (rather than infinitely small

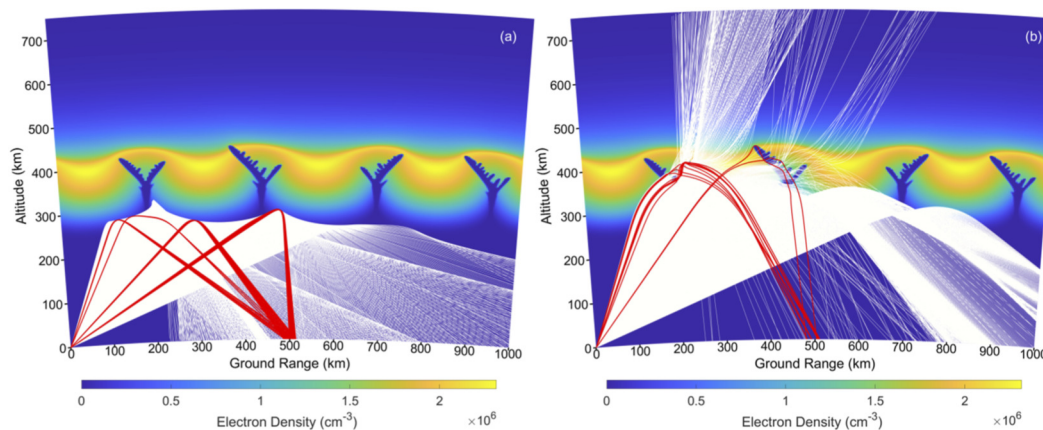


**FIGURE 8** Propagation paths of radio waves with the frequency of 6 MHz (a) and 15 MHz (b) in the ionosphere at  $t = 20.97$  h. Red lines represent the rays received at locations with a ground distance of  $500 \pm 15$  km.

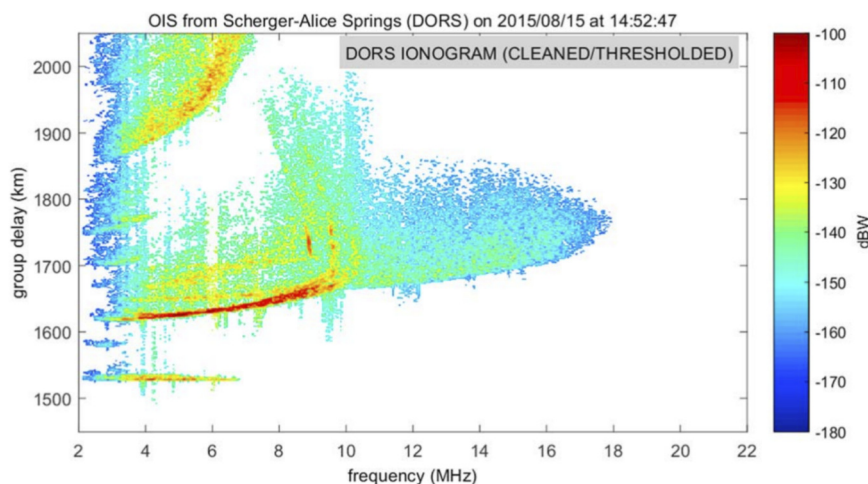


**FIGURE 9** Oblique ionogram measured by DORS (Ayliffe et al., 2019).

elevation angle steps), leading to discrete errors in ray coverage that make it difficult to fully capture the impacts of continuously distributed plasma bubbles in the real ionosphere on radio waves across the entire frequency band.

2. Spread F in the actual ionosphere is induced by plasma bubbles with multi-scale and dynamically evolving characteristics, and these structures exhibit extremely high complexity in terms of electron density fluctuations, spatial morphology, and evolutionary properties, which cannot be accurately replicated by simulation models.
3. Ray-tracing method can only simulate the reflection process of radio waves by plasma bubbles, whereas the formation of spread F across the entire frequency band in observed ionograms is also related to the secondary scattering of radio waves within plasma bubbles. This key physical process is not incorporated into the simulation framework, resulting

in the failure to reproduce spread F in the low-frequency band.

Although ray-tracing method cannot fully simulate the full-band spread F observed in measurements, the propagation paths of high-frequency radio waves are relatively short, making them less affected by discrete elevation angle errors and secondary scattering. Thus, ray-tracing method can still effectively reproduce the spread F characteristics in the high-frequency band, which exhibits good consistency with the measured results.

## 5 Conclusion

In this technical note, we investigated the effects of equatorial plasma bubbles (EPB) on the oblique propagation characteristics

of high-frequency (HF) electromagnetic (EM) waves by means of a two-dimensional model of plasma bubbles and ray-tracing method. Spread F on oblique ionograms and its evolution processes can be reproduced well in this study. Compared with measured oblique ionograms, results show that characteristics of spread F on the synthesized oblique ionograms are consistent with the measured ones. Results verify that the proposed method can effectively study the effects of plasma bubbles on the propagation characteristics of HF oblique waves.

This study holds great reference value for the engineering applications of shortwave communication systems and radar detection. By studying oblique ionograms, we can monitor the occurrence and duration of satellite traces in the ionograms to predict the emergence of small-scale ionospheric perturbations in advance; judge the development stage and influence degree of irregularities through the diffusion range and intensity of the spread F; and then targetedly adjust communication frequencies, optimize transmission elevation angles and power parameters. This can effectively avoid problems such as deflection of radio wave propagation paths and signal amplitude and phase scintillation, reduce the risk of communication interruption or distortion, and ensure the stability and reliability of shortwave communication in the complex ionospheric environment of equatorial and low-latitude regions.

## Data availability statement

The raw data supporting the conclusions of this article will be made available by the authors, without undue reservation.

## Author contributions

ZiZ: Writing – original draft, Methodology, Validation, Visualization, Investigation, Data curation, Formal Analysis. LZ: Investigation, Writing – review and editing, Methodology, Validation. CJ: Validation, Methodology, Writing – review and editing, Supervision, Investigation, Funding acquisition. TL: Formal Analysis, Writing – review and editing, Investigation. GY: Investigation, Writing – review and editing, Formal Analysis. ZhZ: Supervision, Writing – review and editing, Investigation, Formal Analysis.

## References

- Alam, K. E., De Paula, E. R., and Bertoni, F. C. P. (2004). Effects of the fringe field of rayleigh-taylor instability in the equatorial E and valley regions. *J. Geophys. Res. Space Phys.* 109 (A12). doi:10.1029/2003JA010364
- Ankita, M., Tulasi Ram, S., Yokoyama, T., Tsunoda, R. T., Dimri, A. P., Mondal, S., et al. (2025). Satellite traces: Ionogram signatures of bottom-side upwelling structures—a simulation study. *Geophys. Res. Lett.* 52 (7), e2024GL114119. doi:10.1029/2024gl114119
- Ayliffe, J. K., Durbridge, L. J., Frazer, G. J., Gardiner-Garden, R. S., Heitmann, A. J., Prschifka, J., et al. (2019). The DST group high-fidelity, multichannel oblique incidence ionosonde. *Radio Sci.* 54 (1), 104–114. doi:10.1029/2018RS006681
- Booker, H. G., and Wells, H. W. (1938). Scattering of radio waves by the F-region of the ionosphere. *Terr. Magnetism Atmos. Electr.* 43 (3), 249–256. doi:10.1029/TE043i003p00249
- Cervera, M. A., and Harris, T. J. (2014). Modeling ionospheric disturbance features in quasi-vertically incident ionograms using 3-D magnetoionic ray tracing and atmospheric gravity waves. *J. Geophys. Res. Space Phys.* 119 (1), 431–440. doi:10.1002/2013JA019247
- Dungey, J. W. (1956). Convective diffusion in the equatorial F region. *J. Atmos. Terr. Phys.* 9 (5–6), 304–310. doi:10.1016/0021-9169(56)90148-9
- Fejer, B. G., and Kelley, M. C. (1980). Ionospheric irregularities. *Rev. Geophys.* 18 (2), 401–454. doi:10.1029/RG018i002p00401
- Haselgrove, J. (1963). The Hamiltonian ray path equations. *J. Atmos. Terr. Phys.* 25 (7), 397–399. doi:10.1016/0021-9169(63)90173-9
- Huang, C. S., and Kelley, M. C. (1996). Nonlinear evolution of equatorial spread F: 2. Gravity wave seeding of rayleigh-taylor instability. *J. Geophys. Res. Space Phys.* 101 (A1), 293–302. doi:10.1029/95JA02210

## Funding

The author(s) declared that financial support was received for this work and/or its publication. This work was funded by the National Key Research and Development Program of China (2023YFA1009100) and National Natural Science Foundation of China (NSFC 42188101).

## Acknowledgements

We are grateful to the editor and reviewers for their assistance in evaluating this paper.

## Conflict of interest

The author(s) declared that this work was conducted in the absence of any commercial or financial relationships that could be construed as a potential conflict of interest.

## Generative AI statement

The author(s) declared that generative AI was not used in the creation of this manuscript.

Any alternative text (alt text) provided alongside figures in this article has been generated by Frontiers with the support of artificial intelligence and reasonable efforts have been made to ensure accuracy, including review by the authors wherever possible. If you identify any issues, please contact us.

## Publisher's note

All claims expressed in this article are solely those of the authors and do not necessarily represent those of their affiliated organizations, or those of the publisher, the editors and the reviewers. Any product that may be evaluated in this article, or claim that may be made by its manufacturer, is not guaranteed or endorsed by the publisher.

- Huba, J. D., and Joyce, G. (2007). Equatorial spread F modeling: multiple bifurcated structures, secondary instabilities, large density 'bite-outs,' and supersonic flows. *Geophys. Res. Lett.* 34 (7). doi:10.1029/2006GL028519
- Huba, J. D., Joyce, G., and Krall, J. (2008). Three-dimensional equatorial spread F modeling. *Geophys. Res. Lett.* 35 (10). doi:10.1029/2008GL033509
- Jiang, C. H., and Zhao, Z. Y. (2019). Numerical simulation of recombination rate effect on development of equatorial plasma bubbles. *Acta Phys. Sin.* 68 (19), 199401. doi:10.7498/aps.68.20190173
- Jiang, C., Yang, G., Liu, J., and Zhao, Z. (2019). A study of the F2 layer stratification on ionograms using a simple model of TIDs. *J. Geophys. Res. Space Phys.* 124 (2), 1317–1327. doi:10.1029/2018JA026040
- Jiang, C. H., Wei, L. H., Yang, G. B., Zhou, C., and Zhao, Z. (2020). Numerical simulation of the propagation of electromagnetic waves in ionospheric irregularities. *Earth Planet. Phys.* 4 (6), 565–570. doi:10.26464/epp2020059
- Jiang, C., Wei, L., Yokoyama, T., Tian, R., Liu, T., and Yang, G. (2023). Modeling of multi-ion plasma bubbles in the equatorial ionosphere. *J. Geophys. Res. Space Phys.* 128 (10), e2023JA031753. doi:10.1029/2023JA031753
- Jones, R. M. (1968). A three-dimensional ray-tracing computer program (digest of ESSA technical report, ITSA no. 17). *Radio Science* 3 (1), 93–94. doi:10.1002/rds19683193
- Jones, R. M., and Stephenson, J. J. (1975). *A versatile three-dimensional ray tracing computer program for radio waves in the ionosphere*. Washington, DC: US Department of Commerce, Office of Telecommunications.
- Kelley, M. C. (2009). *The earth's ionosphere: plasma physics and electrodynamics*. Academic Press.
- Kudeki, E. (2010). *Applications of radiowave propagation*. USA: University of Illinois at Urbana-Champaign.
- Li, Z., Lei, J., and Zhang, B. (2023). Three-dimensional simulation of equatorial spread F: effects of field-aligned plasma flow and ionospheric conductivity. *J. Geophys. Res. Space Phys.* 128 (3), e2022JA031070. doi:10.1029/2022JA031070
- Ma, X., Guo, P., and Wu, M. (2023). Simulation research on the influence of plasma bubbles on radio wave propagation. *Radio Sci.* 58 (2), 1–16. doi:10.1029/2022rs007577
- Mathur, N. C., and Pandey, R. P. (1977). Ray tracing study of effects of ionospheric irregularities on HF and VHF radio waves. *IETE J. Res.* 23 (3), 121–123. doi:10.1080/03772063.1977.11451283
- Ossakow, S. L. (1981). Spread-F theories-A review. *J. Atmos. Terr. Phys.* 43 (5-6), 437–452. doi:10.1016/0021-9169(81)90107-0
- Paul, A. K., Smith, G. H., and Wright, J. W. (1968). Ray-tracing synthesis of ionogram observations of a large local disturbance in the ionosphere. *Radio Sci.* 3 (1), 15–26. doi:10.1002/rds19683115
- Song, H., Qing, H., and Zou, X. (2022). A parallel optimization 3D numerical ray-tracing method for the fast and accurate simulation of disturbed oblique ionogram. *Adv. Space Res.* 70 (10), 2894–2904. doi:10.1016/j.asr.2022.07.052
- Tsunoda, R. T. (2008). Satellite traces: an ionogram signature for large-scale wave structure and a precursor for equatorial spread F. *Geophys. Res. Lett.* 35 (20). doi:10.1029/2008GL035706
- Yokoyama, T., Shinagawa, H., and Jin, H. (2014). Nonlinear growth, bifurcation, and pinching of equatorial plasma bubble simulated by three-dimensional high-resolution bubble model. *J. Geophys. Res. Space Phys.* 119 (12), 474. doi:10.1002/2014JA020708
- Zalesak, S. T., and Ossakow, S. L. (1980). Nonlinear equatorial spread F: spatially large bubbles resulting from large horizontal scale initial perturbations. *J. Geophys. Res. Space Phys.* 85 (A5), 2131–2142. doi:10.1029/JA085iA05p02131
- Zalesak, S. T., Ossakow, S. L., and Chaturvedi, P. K. (1982). Nonlinear equatorial spread F: the effect of neutral winds and background Pedersen conductivity. *J. Geophys. Res. Space Phys.* 87 (A1), 151–166. doi:10.1029/JA087iA01p00151